March, 1995

Three-dimensional location estimation of trajectories of point targets using a projection-based transformation method

Jae-Ho Choi, *Chonbuk National University*
Sarah A. Rajala, *North Carolina State University*

Three-dimensional location estimation of trajectories of point targets using a projection-based transformation method

Jae-Ho Choi
Chonbuk National University
Department of Computer Engineering
Chonju, Chonbuk, 560-756, Korea
E-mail: jchoi@mips.chonbuk.ac.kr

Sarah A. Rajala
North Carolina State University
Department of Electrical and Computer Engineering
Campus Box 7911
Raleigh, North Carolina 27695-7911

Abstract. A new computational approach for determining the parameters that characterize the locations of trajectories of point targets in a 3-D space is described. The targets of concern are dim, unresolved point targets moving along straight paths across the same field of view. Since the target's signal-to-noise ratio is low and the spatial extent of the target is less than a pixel, one must rely on integration over a target track that spans many image frames. The proposed method estimates these parameters by transforming the entire set of time-sequential images of a constant field of view into the projection space by using a modified Radon transform. Since the 3-D (spatiotemporal) data can be decomposed into 2-D multiple-view representations along arbitrary orientations, the Radon transform enables us to analyze the 3-D problem in terms of its 2-D projections. When this generalization of the Hough transform-based algorithm using the Radon transform is applied to a set of real infrared images, it produces promising estimation results even under noisy conditions. The noise in the images is assumed to be additive white Gaussian.

Subject terms: target motion detection/estimation; Radon transform; Hough transform; computer vision; remote sensing.

Optical Engineering 34(3), 933-939 (March 1995).

1 Introduction

Remote sensing of small moving objects in a time-sequential set of digital image data is a problem that has received much attention in recent years. Examples include ground-based sensing of satellites, meteors, and asteroids and detection of airborne targets such as aircraft in satellite-acquired imagery.[1–3] This paper is directed toward the last example, tracking a small, dim moving target in a three-dimensional (two spatial and one temporal) space. Image data acquired using a focal-plane array of infrared or optical sensors is often used. The sensor array collects a time-sequential set of two-dimensional image frames, each of which contains background clutter, noise from the electronics, and targets, if present. Although the target size varies—depending on the actual target size, the satellite platform altitude, the target speed, and the optics—of particular interest in this work are targets whose size is on the order of one pixel.

In any one frame, however, it is difficult to distinguish a target from the background and noise, because the target is small and may be dim. Since the sensor collects each image frame periodically and the target is moving, the target track appears in a set of spatiotemporal 3-D data as a straight line or other curve. The motion of the target against the relatively static background is one of the main features that distinguish the target from the background; thus a target can be detected and tracked by extracting its trajectory from the background and the noise. For satellite imagery, it is reported that frame registration is possible to the 0.1-pixel level.[4] Because a target's position changes much faster than that of the background, temporal filtering is most advantageous if background changes are not too severe. After preprocessing, the 3-D data set is typically processed further to increase the effective target signal-to-noise ratio by integrating along the target trajectory. One common method is to project the 3-D data along the temporal axis onto a plane defined by two spatial axes (x and y) to create the so-called track map.[5] Depending on the target speed, the accentuated trajectory in the track map appears as a straight line or some other curve; hence the target trajectory can then be estimated using a method such as the Hough transform.[6,7] Unfortunately, there is a problem with using a projection to create a 2-D image from the 3-D data. The projection usually causes a reduction in the effective signal-to-noise ratio from that of the original

Paper 08083 received Aug. 7, 1994; revised manuscript received Sep. 3, 1994; accepted for publication Sep. 3, 1994.

3-D data. One approach to overcoming this problem is to use the original 3-D volume of data as a whole.[8–10]

In this paper, we present a projection-based transformation method derived from the Radon transform as an alternative approach to estimating the location of the 3-D target trajectory. The Radon transform produces a set of $(N-1)$-dimensional projections from an N-dimensional function. Although there is an increase in the number of computations needed to compute the projections, by taking a set of projections at arbitrary orientations, it can effectively increase the track estimation capability. In other words, by taking a number of 2-D projections from the entire set of 3-D data, we can decompose the 3-D spatiotemporal data into 2-D multiple-view representations along arbitrary orientations. This enables us to analyze the 3-D problem in terms of 2-D projections and allows us to reconstruct the estimated 3-D target trajectory in the original spatiotemporal space using back projection.

The paper is organized as follows. Section 2 contains a description of the fundamental theories related to the projection-based transformation method. Section 3 contains a description of the proposed method that utilizes a modified version of the Radon transform and 2-D line tracking using the Hough transform. The backward projection scheme for 3-D reconstruction is also included. Finally, the results of the computer simulation follow in Section 4.

2 Fundamental Theory

In this section the Radon transform is described as a basis for the projection method. Introduced early in the twentieth century,[11] the Radon transform theory has demonstrated its usefulness in applications for pattern recognition and feature extraction,[12] nuclear medicine and imaging by magnetic resonance,[13] and geophysics and seismographics.[14] Fundamental to most of these applications is that the Radon transform enables feature extraction and classification at high speed by converting N-dimensional computation to a sequence of $(N-1)$-dimensional operations.[15] For example, given a sequence of images (3-D data), the Radon transform relieves the system's computational bottleneck by keeping the efficient feature extraction operations in a number of 2-D Radon planes.

Although the Radon transform can be defined for any N-dimensional general function,[16] in this paper the special cases of the 2-D and 3-D Euclidean (or image) space are considered. Computing the Radon transform consists in computing the projections of an image along a particular pattern, e.g., a straight line or a plane. Mathematically, the problem can be stated as follows. Let $G(x,y)$ represent a 2-D general function. As shown in Fig. 1, a line running through $G(x,y)$ is called a *ray*. The integral of $G(x,y)$ along a ray is called a *ray integral,* and a set of ray integrals forms a *projection.* The equation for an individual ray is given by

$$\kappa = y\cos\phi - x\sin\phi \tag{1}$$

where κ is the perpendicular distance of the ray from the origin. The integral of the function $G(x,y)$ along this ray may be expressed as

$$R(\kappa;\phi) = \int_{\text{ray}} G(x,y)\ \mathrm{d}^2 r = \int_{-\infty}^{\infty}\int_{-\infty}^{\infty} G(x,y)$$

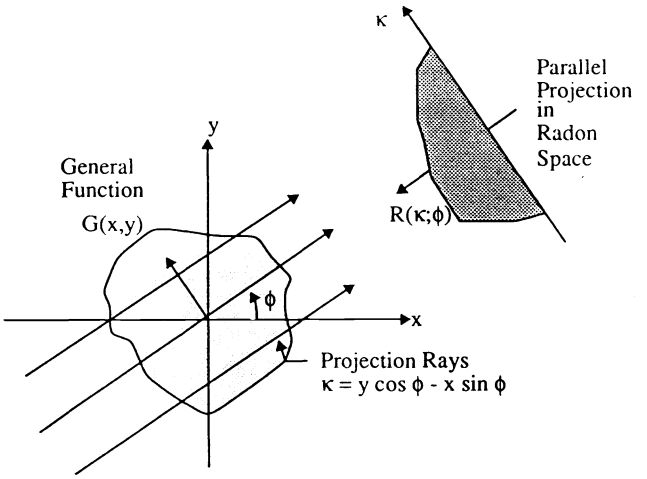

Fig. 1 Geometry for the 2-D Radon transform.

$$\times\,\delta(\kappa - y\cos\phi + x\sin\phi)\ \mathrm{d}x\ \mathrm{d}y\ , \tag{2}$$

where $R(\kappa;\phi)$ as a function of κ is the parallel projection of $G(x,y)$ at angle ϕ. The set of 1-D functions $R(\kappa;\phi)$ is called the Radon transform of $G(x,y)$. The entire 2-D distribution $R(\kappa;\phi)$ taken along a set of parallel rays, defined in Eq. (1), is referred to as the *parallel projection* data.

The projection data are often represented in a format referred to as a sinogram, which is indexed by the variables κ and ϕ. To illustrate this, consider a unit-intensity point at (x_0,y_0). From Eq. (1),

$$\begin{aligned}\kappa &= y_0\cos\phi - x_0\sin\phi\\ &= \sqrt{x_0^2+y_0^2}\,\cos[\phi + \tan^{-1}(y_0/x_0)]\ .\end{aligned} \tag{3}$$

Each point in image space maps to a sinusoidal curve in Radon space whose amplitude and phase are given in Eq. (3). The value along this sinusoid is the value of the point at (x_0,y_0). The sinogram is just the summation of weighted sinusoids due to a collection of points in the image space. The Radon transform in this format is closely related to the Hough transform, which is a line and curve detection technique. The related literature on the Radon transform and its relationship to the Hough transform can be found in Ref. 17.

Similarly to the 2-D Radon transform, a general 3-D function of (x,y,t) can be decomposed into a set of 2-D projection planes that are parametized by an arbitrary two-component vector. Mathematically, the 3-D Radon transform can be written as

$$R(\kappa;\mathbf{n}) = \int_{-\infty}^{\infty}\int_{-\infty}^{\infty}\int_{-\infty}^{\infty} G(\mathbf{x})\delta(\kappa - \mathbf{x}\cdot\mathbf{n})\ \mathrm{d}^3\mathbf{x} \tag{4}$$

for a three-dimensional volume (or object) $G(\mathbf{x})$, where $\mathbf{x} = [x,y,t]$, $R(\kappa;\mathbf{n})$ denotes the surface integral of $G(\mathbf{x})$ over the plane $\kappa = \mathbf{x}\cdot\mathbf{n}$, $\mathbf{n} = [n_1,n_2,n_3]$ denotes a unit vector normal to the plane, and κ is the distance of the plane from the origin. The Radon problem is to determine $G(\mathbf{x})$ given the set of integrals $R(\kappa;\mathbf{n})$ for all κ and n. The geometry of the problem is illustrated in Fig. 2, from which

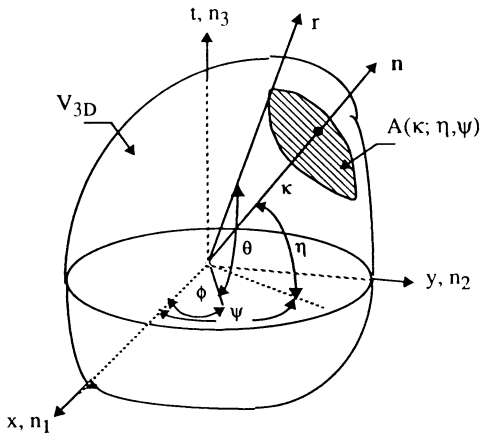

Fig. 2 Geometry for the 3-D Radon transform.

$$\mathbf{x} \equiv [x,y,t] = [r \cos\theta \cos\phi,\ r \cos\theta \sin\phi,\ r \sin\theta] \ , \tag{5}$$

$$\mathbf{n} \equiv [\cos\eta \cos\psi,\ \cos\eta \sin\psi,\ \sin\eta] \ , \tag{6}$$

$$G(\mathbf{x}) = G(x,y,t) = G(r,\theta,\phi) = \begin{cases} 1 & \text{if } \mathbf{x} \in V_{3\text{-D}} \ , \\ 0 & \text{otherwise} \ . \end{cases} \tag{7}$$

Using Eqs. (4) to (7), the 3-D Radon transform of $G(x,y,t)$ can be expressed as

$$R(\kappa;\eta,\psi) = \int_0^{\infty}\int_0^{2\pi}\int_{-\pi/2}^{\pi/2} G\delta(\kappa - r[\cos\theta \cos\eta \times \cos(\phi-\psi) + \sin\theta \sin\eta])r^2 \cos\theta \, d\theta \, d\phi \, dr \ , \tag{8}$$

where $R(\kappa;\eta,\psi)$ is just the cross-sectional area $A(\kappa;\eta,\psi)$ of the body as a function of the direction of viewing (η,ψ), and κ is the distance from the origin. Thus, knowing the areas of $A(\kappa;\eta,\psi)$ for all κ and (η,ψ), one can obtain G in terms of the cross-sectional area of the body[18]:

$$G(r,\theta,\phi) = -\frac{1}{8\pi^2}\int_0^{2\pi}\int_{-\pi/2}^{\pi/2}\left[\frac{\partial^2 A(\kappa;\eta,\psi)}{\partial\kappa^2}\right]_{\kappa} \cos\eta \, d\eta \, d\psi \ , \tag{9}$$

where $\kappa = r[\cos\theta \cos\eta \cos(\phi-\psi) + \sin\theta \sin\eta]$.

In the next section, the generalized Hough-transform-based projection method using the Radon transform is described. Here, the transformation geometry becomes relatively simple because we are dealing with straight lines in the 3-D spatiotemporal image space.

3 Generalized Projection-Based Method

In our generalized projection-based algorithm the Radon transform provides a mechanism for obtaining the projections at arbitrary orientations. In our approach, however, the Radon transform is modified into a simpler form utilizing the symmetry, aligning the aspects of the projection, and incorporating the maximum-value projection scheme.[19] As shown in Fig. 3, the modified Radon transform can be written as follows:

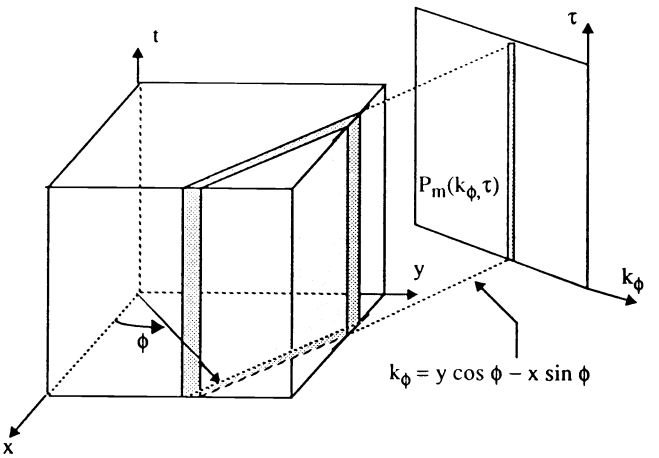

Fig. 3 Geometry for the modified 3-D Radon transform.

$$P_m(\kappa_\phi,\tau) = \max_{t=0}^{N-1} T(x,y,t)\delta(\kappa_\phi - y \cos\phi + x \sin\phi) \ , \tag{10}$$

where the projections are taken along

$$\kappa_\phi = y \cos\phi - x \sin\phi \ . \tag{11}$$

For the 3-D volume of image data composed of N time-sequential frames with a possible target trajectory $T(x,y,t)$, we let $P_m(\kappa_\phi,\tau)$ denote a set of parallel projections taken along a series of parallel projection planes defined by the Dirac delta function of Eq. (11). The series of projection planes in this case is perpendicular to the xy plane. As a function of κ_ϕ and τ for a given value of ϕ, $P_m(\kappa_\phi,\tau)$ will be referred to as the parallel projection of $T(x,y,t)$ for angle ϕ.

In order to take full advantage of the Radon transform and the straight-line geometry of the target trajectory, we could take another set of projections along the series of projection planes that are perpendicular to the yt plane. By changing Eq. (11) to

$$\kappa_\gamma = t \cos\gamma - y \sin\gamma \tag{12}$$

another unique set of projections can be obtained as follows:

$$P_m(\kappa_\gamma,\nu) = \max_{x=0}^{L-1} T(x,y,t)\delta(\kappa_\gamma - t \cos\gamma + y \sin\gamma) \ , \tag{13}$$

where L is the spatial resolution of the digital image data. For simplicity of formulation, although the image can be of any size, we have assumed that the image is an $L \times L$ square. The visualization of Eq. (13) is similar to what is given in Fig. 3. It is evident that in our projection-based transformation the temporal-axis index t and the projection space index τ are equivalent geometrically. A similar equivalence can be seen for the indices x and ν in Eq. (13). In addition, both of the projection angles ϕ and γ are assumed to be within the range from 0 to 90 deg.

For an arbitrary number of projections in the data, given the numbers of projections for the two orientations C_ϕ and C_γ, respectively, the projection angles ϕ and γ are defined as follows:

$$\phi = i\ \Delta\phi \qquad \text{for} \quad i = 0,1,\ldots,C_\phi - 1 \tag{14}$$

and

$$\gamma = j\ \Delta\gamma \qquad \text{for} \quad j = 0,1,\ldots,C_\gamma - 1\ , \tag{15}$$

where

$$\Delta\phi = \frac{90\ \text{deg}}{C_\phi - 1} \tag{16}$$

and

$$\Delta\gamma = \frac{90\ \text{deg}}{C_\gamma - 1}\ . \tag{17}$$

Once the total of $C_\phi + C_\gamma$ parallel projections are obtained using Eqs. (10)–(17), the target track parameters for each one of the projections are estimated by using the straight-line-finding 2-D Hough transform. The straight line in the Cartesian coordinate (image space) system can be parameterized in several ways, depending on the application. In this paper, we have used the normal parametrization as follows:

$$\rho_0 = x\ \cos\theta_0 + y\ \sin\theta_0\ , \tag{18}$$

where ρ_0 is the normal distance from the line to the origin, and θ_0 is the angle of the normal line with respect to the x axis. Equation (18) defines a transformation from the image space to the Hough parameter space in which the coordinate axes are indexed by the Hough-space parameters ρ and θ as shown in Fig. 4. The $\rho\theta$ Hough parameter space, which is implemented as an accumulator array in which each bin represents a quantized value of ρ and θ, is incremented wherever the sinusoidal curve corresponding to an image point passes through the specific set of points of the $\rho\theta$ plane corresponding to its (ρ,θ) values. At the end of the accumulation process, if a peak in the Hough parameter space is detected, a line is assumed and its location is given by the (ρ,θ) values associated with the accumulator array bin.

In the final stage, the estimate of the 3-D target trajectory in the original 3-D image space is then obtained by back-projecting the tracks estimated for each one of the projections, i.e., $(\bar{\rho}_i,\bar{\theta}_i)$ for $i = 0,1,\ldots,C_\phi - 1$, and $(\bar{\rho}_j,\bar{\theta}_j)$ for $j = 0,1,\ldots,C_\gamma - 1$. The backward projection for the 3-D reconstruction, as shown in Fig. 5, is expressed as follows:

$$\bar{T}(x,y,t) = \sum_{i=0}^{C_\phi - 1} \bar{T}_i(\kappa_\phi,\tau)\delta(\kappa_\phi - y\ \cos\phi + x\ \sin\phi) + \sum_{j=0}^{C_\gamma - 1} \bar{T}_j(\kappa_\gamma,\nu)\delta(\kappa_\gamma - t\ \cos\gamma + y\ \sin\gamma)\ , \tag{19}$$

where $\bar{T}_i(\kappa_\phi,\tau)$ and $\bar{T}_j(\kappa_\gamma,\nu)$ are the estimated 2-D target track functions obtained by the 2-D inverse Hough transformation for $C_\phi + C_\gamma$ projections taken along projection angles ϕ and γ, respectively.

$$\bar{T}_i(\kappa_\phi,\tau) = \bar{\rho}_i - \kappa_\phi\ \cos\bar{\theta}_i - \tau\ \sin\bar{\theta}_i = 0 \quad \text{for} \quad i = 0,\ldots,C_\phi - 1 \tag{20}$$

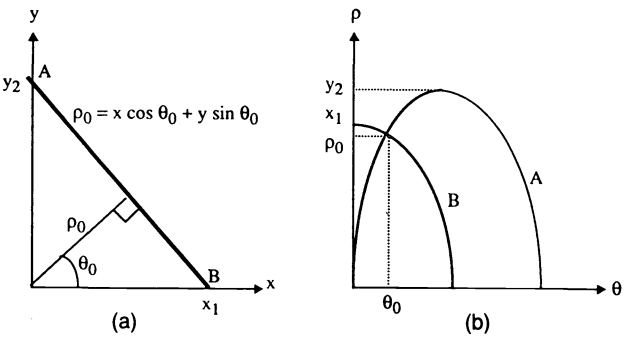

Fig. 4 Mapping between the image space and the Hough-parameter space: (a) points *A* and *B* in the image space are mapped to (b) curves *A* and *B* in the Hough-parameter space. The line in (a) maps to a point (ρ_0,θ_0) in (b).

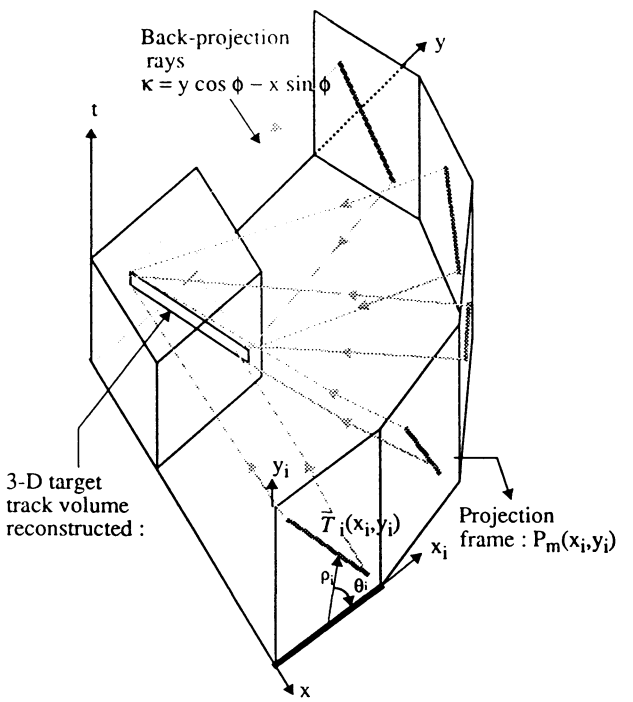

Fig. 5 Estimated 3-D track reconstruction using a backward projection.

and

$$\bar{T}_j(\kappa_\gamma,\nu) = \bar{\rho}_j - \kappa_\gamma\ \cos\bar{\theta}_j - \nu\ \sin\bar{\theta}_j = 0 \quad \text{for} \quad j = 0,\ldots,C_\gamma - 1\ . \tag{21}$$

Then $\bar{T}(x,y,t)$, after thresholding, is the reconstructed 3-D target trajectory function. The backward projection hence can be viewed as an accumulation of extracted features found in the projection space onto the original spatiotemporal 3-D image space. In our case, the 2-D straight-line track features estimated in the projections were accumulated backward along the parallel projection planes and created the volume of the reconstructed 3-D track estimate. The convergence of 3-D track estimation from the projection data is limited by the input image signal-to-noise ratio and the discretization

errors (data sampling and quantization). Discretization errors occur when the data are recorded discretely and when there is a projection onto a plane that is not parallel to one of three coordinate axes.

In the next section we present the simulation results for the generalized projection-based transformation method for estimating 3-D (spatiotemporal) locations of trajectories traveled by unresolved targets. The simulations are performed using the set of real infrared image data.

4 Simulation Results

Simulations were done to demonstrate the performance of our projection-based transformation method for estimating the tracks of unresolved targets using the real infrared unclassified data provided by the Naval Research Laboratory (HiCamp data shown in Fig. 6). The primary target track geometry consists of nonmaneuvering straight lines. The objective is to study the behavior of our projection-based tracking system as a function of the number of projections, the signal-to-noise ratios, and the number of image frames. Each data set has a frame size of 32×32 pixels and up to 46 frames in the temporal direction to accommodate the longest possible track of a target moving at a speed of one pixel per frame. Since an image sequence with a real target in the scene was not available, the point targets were synthetically generated and superimposed into the time-sequential set of data with a variable amount of white, Gaussian noise, denoted by N. Under the assumption that a target has a spatial extent of less than a pixel, the targets were added as follows:

$$I_{x,y,t} = \begin{cases} \alpha C + (1-\alpha) B_{x,y,t} + N \ , & x,y,t \in T(x,y,t) \ , \\ B_{x,y,t} + N & \text{otherwise} \ , \end{cases} \tag{22}$$

where $T(x,y,t)$ is the trajectory function embedded in the image data $I_{x,y,t}$, $B_{x,y,t}$ is the image background intensity, and C is the target intensity. The variable α $(0 \le \alpha \le 1)$ controls the contribution of the target to the pixel; for $\alpha = 1$, the target covers the whole pixel.

Given the image sequence model of Eq. (22), the target signal-to-noise ratio (SNR) is defined as follows:

$$\mathrm{SNR} = 10 \ \log_{10}\left(\frac{(\alpha^2/M) \sum_{x,y,t \in T(x,y,t)} (C - B_{x,y,t})^2}{\sigma_N^2} \right) \ , \tag{23}$$

where M is the total number of image frames in the 3-D data, and σ_N^2 is the noise variance.

A number of simulation runs have been made using the projection-based track localization algorithm. For many of the simulations the target locations are estimated early in their trajectories with 15 data frames or less. Three of the more difficult cases are presented in Table 1, Table 2, and Table 3, respectively. These three runs are "worst cases" using a 45% ($\alpha = 0.45$) target contribution.

Table 1 summarizes the first target simulation, where the correct trajectory is at $\rho = 26$, $\theta = 45$ deg, and $t = 0$. When this trajectory is expressed in terms of the spatiotemporal 3-D motion vector, the target moves with the motion vector $(1.0, -1.0, 1.0)$ in the x, y, and t directions, respectively. For SNRs above 10.0 dB, most of the good estimates of ρ and θ are found within 20-data-frame time (FRM = 20), while for

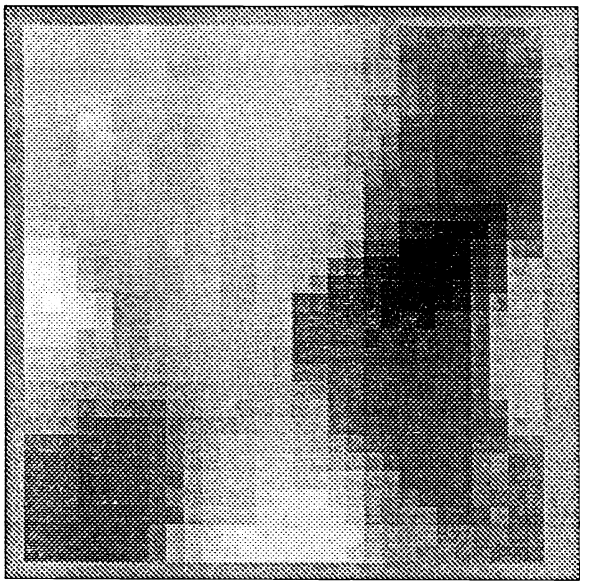

Fig. 6 The HiCamp background data.

Table 1 The 3-D track parameter estimation of a target using HiCamp: the target has the true 3-D motion vector $(1.0, -1.0, 1.0)$ in the x, y, and t directions, respectively, and the 2-D Hough-space parameters $\rho = 26$, $\theta = 45$ deg. In the table, PROJ = total number of projections, FRM = number of data frames, SNR = signal-to-noise ratio, 3-D = 3-D spatiotemporal motion vector estimation, and HP = 2-D Hough space parameters estimated.

PROJ	FRM	SNR = 16.7 dB		SNR = 13.7 dB	
		3-D	HP	3-D	HP
3	16	1.0, -0.24, 0.33	28, 80°	1.0, 1.05, 0.15	1, 316°
	19	1.0, -1.09, 0.94	26, 43°	1.0, -1.06, 1.00	26, 43°
	22	1.0, -0.95, 0.89	26, 46°	1.0, -0.96, 0.71	26, 46°
	25	1.0, -1.03, 0.92	26, 44°	1.0, -1.03, 0.92	26, 44°
5	16	1.0, -0.24, 0.33	28, 80°	1.0, 1.05, 0.03	1, 316°
	19	1.0, -1.19, 0.94	26, 43°	1.0, -1.06, 0.98	26, 43°
	22	1.0, -0.95, 0.89	26, 46°	1.0, -0.95, 0.71	26, 46°
	25	1.0, -1.03, 0.92	26, 44°	1.0, -1.03, 0.94	26, 44°
		SNR = 10.7 dB		SNR = 9.10 dB	
3	16	1.0, 1.03, 0.03	1, 316°	1.0, 1.02, 0.14	1, 316°
	19	1.0, -1.18, 0.51	26, 41°	1.0, -1.18, 0.51	26, 41°
	22	1.0, -0.96, 0.71	26. 46°	1.0, -0.95, 0.28	26, 46°
	25	1.0, -0.96, 0.90	26, 46°	1.0, -0.96, 0.90	26, 49°
5	16	1.0, 1.03, 0.12	1, 316°	1.0, 1.13, 0.25	1, 51°
	19	1.0, -1.19, 0.44	26, 41°	1.0, -1.09, 0.44	26, 43°
	22	1.0, -0.95, 0.72	26, 46°	1.0, -0.95, 0.27	26, 46°
	25	1.0, -0.96, 0.89	26, 46°	1.0, -0.96, 0.89	26, 49°

the 3-D motion vector of the target, good estimates are found within 25 frames. The tracking performance, however, did not increase appreciably when the number of projections (PROJ) was increased from three to five. For PROJ = 3, the projections are taken along x, y, and t coordinate axes, i.e., $\phi = 0$, 90 deg and $\gamma = 0$ deg; for PROJ = 5, two additional projections are taken along $\phi = 45$ deg and $\gamma = 45$ deg. Figure 7 shows the 3-D reconstruction of the estimated target trajectory for PROJ = 3, FRM = 25, and SNR = 11.9 dB. The estimated 3-D motion vector is $(1.00, -0.96, 0.90)$, with the corresponding Hough-parameter estimates $\rho = 26$, $\theta = 46$ deg, and $t = 24$. The reconstructed trajectory is found on average 0.82 pixels away from the actual trajectory.

The second simulation is for the trajectory at $\rho = 4$, $\theta = 135$ deg, and $t = 0$, in which the target moves with the 3-D motion

Table 2 The 3-D track parameter estimation of a target using HiCamp: the target has the true 3-D motion vector (1.0,1.0,1.0) in *x*, *y*, and *t* directions, respectively, and the 2-D Hough-space parameters $\rho = 4$, $\theta = 135$ deg.

PROJ	FRM	SNR = 17.5 dB		SNR = 14.3 dB	
		3-D	HP	3-D	HP
3	16	1.00, 0.95, 0.95	4,135°	1.00, 1.11, 0.33	5,138°
	19	1.00, 1.02, 0.46	4,136°	1.00, 1.02, 0.46	4,136°
	22	1.00, 1.00, 1.00	4.136°	1.00, 1.00, 1.00	4,136°
	25	1.00, 1.00, 1.00	4,136°	1.00, 1.01, 0.97	4,136°
5	16	1.00, 0.95, 0.95	4,135°	1.00, 1.11, 0.33	4,138°
	19	1.00, 1.00, 1.00	4,136°	1.00, 1.00, 1.00	4,136°
	22	1.00, 1.00, 1.00	4,136°	1.00, 1.00, 1.00	4,136°
	25	1.00, 1.00, 1.00	4,136°	1.00, 1.01, 0.97	4,136°
		SNR = 12.7 dB		SNR = 11.3 dB	
3	16	1.00, 1.71, 0.25	10,135°	1.00, -0.61, -0.37	23, 69°
	19	1.00, 1.02, 0.46	4,136°	1.00, 0.48, 0.16	8,115°
	22	1.00, 1.03, 0.58	4,137°	1.00, 0.98, 0.57	6,133°
	25	1.00, 1.01, 0.97	4,136°	1.00, 0.98, 0.96	4,135°
5	16	1.00, 0.28, 0.27	9,106°	1.00, -0.61, -0.37	23, 69°
	19	1.00, 1.00, 0.46	4,136°	1.00, 0.48, 0.16	8,115°
	22	1.00, 1.03, 0.58	4,137°	1.00, 0.98, 0.58	6,133°
	25	1.00, 1.01, 0.97	4,136°	1.00, 1.01, 0.97	4,135°

Table 3 The 3-D track parameter estimation of a target using HiCamp: the target has the true 3-D motion vector (1.0, −0.5,1.0) in *x*, *y*, and *t* directions, respectively, and the 2-D Hough-space parameters $\rho = 14$, $\theta = 64$.

PROJ	FRM	SNR = 18.0 dB		SNR = 15.0 dB	
		3-D	HP	3-D	HP
3	16	1.00, -0.49, 0.95	14, 64°	1.00, -0.57, -0.26	14, 61°
	19	1.00, -0.52, 1.01	14, 62°	1.00, -0.52, 1.01	14, 62°
	22	1.00, -0.49, 0.97	14, 64°	1.00, -0.49, 1.02	14, 64°
	25	1.00, -0.52, 1.01	14, 63°	1.00, -0.52, 1.01	14, 63°
5	16	1.00, -0.49, 0.95	14, 64°	1.00, -0.56, -0.27	14, 61°
	19	1.00, -0.52, 1.01	14, 62°	1.00, -0.52, 1.01	14, 62°
	22	1.00, -0.41, 0.97	14, 63°	1.00, -0.49, 1.00	14, 64°
	25	1.00, -0.52, 0.99	14, 63°	1.00, -0.52, 0.99	14, 63°
		SNR = 12.8 dB		SNR = 11.6 dB	
3	16	1.00, -0.49, -0.25	26, 53°	1.00, -0.57, -0.26	26, 53°
	19	1.00, -0.52, 1.01	14, 61°	1.00, -0.52, 1.01	14, 63°
	22	1.00, -0.49, 0.97	14, 64°	1.00, -0.49, 1.02	14, 63°
	25	1.00, -0.52, 1.01	14, 63°	1.00, -0.52, 1.01	14, 64°
5	16	1.00, -0.49, -0.25	26, 53°	1.00, -0.56, -0.26	26, 53°
	19	1.00, -0.52, 1.01	14, 61°	1.00, -0.52, 1.01	14, 63°
	22	1.00, -0.41, 0.97	14, 63°	1.00, -0.49, 1.00	14, 63°
	25	1.00, -0.52, 0.99	14, 63°	1.00, -0.52, 0.99	14, 64°

vector (1.0,1.0,1.0). The results are summarized in Table 2. For SNRs higher than 12.0 dB all of the good 2-D Hough-parameter estimates are obtained within less than 20 data frames. As the SNR dipped below 12.0 dB, the parameter estimation became difficult and required more data frames. At SNR = 11.3 dB the tracking system required 25 data frames to produce a good set of parameter estimates. The performance increase due to the increase in the number of projections from three to five was marginal.

For the third simulation, the trajectory at $\rho = 14$, $\theta = 64$ deg, and $t = 0$ was tested. Here, the target moves with the 3-D motion vector (1.0, − 0.5,1.0) in the *x*, *y*, and *t* directions, respectively. Table 3 shows the simulation results for the SNR values from 18.0 to 11.6 dB. Both of the 2-D Hough-space parameters and the 3-D motion vector estimates are good within 19 data frames throughout the table. As in the two previous simulations, data from more than three projections were found to be redundant.

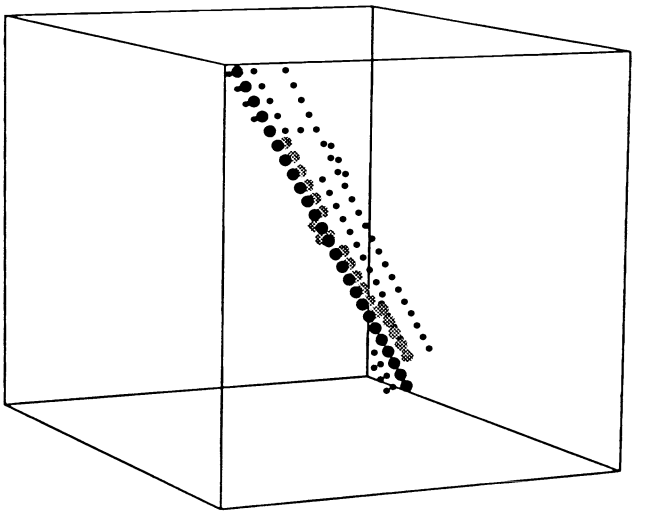

Fig. 7 The 3-D reconstruction of the estimated trajectory.

From the simulations it was found that for good parameter estimation three projections taken parallel to three coordinate axes are adequate for most of the cases, and taking more projections would not increase the estimation performance appreciably.

All these experiments were performed under the assumption that the HiCamp data themselves are noiseless. Additive white noise, as defined in Eq. (22), was synthetically generated and added to the HiCamp image sequence data in order to obtain the desired signal-to-noise ratios. Since it is likely that the inherent noise might be involved during the data acquisition time of the HiCamp data, we have actually been dealing with noisier cases in the simulation runs than those of the SNRs specified above. Inherent-noise analysis of the HiCamp data, however, is outside the scope of this paper. Projection-based algorithm analysis for the real noise cases may be considered for future research.

5 Conclusions

The focus of this paper has been on the 3-D track parameter estimation of small, dim, moving targets embedded in a sequence of digital images, utilizing the modified Radon transform. The theoretical aspects of the Radon transform as a projection mechanism were investigated. This provided a basis for the 3-D projection-based transformation trajectory localization algorithm. The simulations using the HiCamp real infrared data were run to test the performance of the proposed algorithm. The results show that the spatiotemporal 3-D target trajectory estimation is possible down to 9.0 dB within a time of 25 data frames. For most of the cases, the number of projections taken along both of ϕ and γ was found to be three. Furthermore, except for the time required to compute the forward and backward projections, the amount of data to be processed can be reduced significantly. Since these projections are basically orthogonal projections, the technique further enables 3-D target trajectory estimation and reconstruction in real time.

References

1. N. C. Mohanty, "Computer tracking of moving point targets in space," *IEEE Trans. Pattern Anal. and Machine Intell.* **3,** 606–611 (1981).

2. S. C. Pohlig, "Algorithm for detection of moving optical targets," *IEEE Trans. Aero. and Electr. Systems* **AES-25**(1), 56–62 (Jan. 1989).
3. S. A. Rajala, L. W. Nolte, and J. V. Aanstoos, "Detection of unresolved target tracks in infrared imagery," in *Proc. SPIE-VCIP 91, Proc. SPIE* **1606,** 360–371 (Nov. 1991).
4. C. A. Berenstein, L. N. Kanal, and E. C. Olson, "A geometric approach to subpixel registration accuracy," *Computer Vision, Graphics, and Image Processing* **40,** 334–360 (1987).
5. A. E. Cowart, W. E. Snyder, and W. H. Ruedger, "The detection of unresolved targets using the Hough transform," *CVGIP* **21,** 222–238 (1983).
6. P. V. C. Hough, "Method and means for recognizing complex patterns," U.S. Patent No. 3069654 (1962).
7. J. Illingworth and J. Kittler, "A survey of the Hough transform," *CVGIP* **44,** 87–116 (1988).
8. D. J. Hunt, L. W. Nolte, and W. H. Ruedger, "Performance of the Hough transform and its relationship to statistical detection theory," *CVGIP* **43**(2), 221–238 (Aug. 1988).
9. D. J. Hunt, "Performance of the Hough transform and signal detection theory for detection and tracking of dim, moving targets," PhD Thesis, Duke Univ., 1990.
10. D. Jalihal and L. W. Nolte, "Signal detection theory approach to the multiple parallel moving targets," *CVGIP: Graphical Models and Image Process.* **55**(4), 235–254 (July 1993).
11. J. Radon, "Über die Bestimmung von Funktionen durch ihre Intervalwerte längs gewisser Mannigfaltigkeiten (On the determination of functions from their integrals along certain manifolds)," *Ber. Sächs. Akad. Wiss. Leipzig Math.-Phys. Klass* **69,** 262–277 (1917).
12. G. R. Gindi and A. F. Gmitro, "Optical feature extraction via the Radon transform," *Opt. Eng.* **23**(5), 499–506 (1984).
13. G. Herman, *Image Reconstruction from Projections—the Fundamentals of Computerized Tomography,* Academic, New York (1980).
14. A. J. Devaney, "Geophysical diffraction tomography," *IEEE Trans. Geosci. Remote Sensing* **22**(1), 3–13 (1984).
15. G. Belykin, "Discrete Radon transform," *IEEE Trans. Acoust. Speech Signal Process.* **35**(2), 162–172 (1987).
16. I. M. Gel'fand, M. I. Graev, and N. Y. Vilenkin, *Generalized Functions,* Academic, New York, 1966.
17. S. R. Dean, "Hough transform from Radon transform," *IEEE Trans. Pattern Anal. and Machine Intell.* **PAMI-3,** 185–188 (Mar. 1981).
18. R. M. Lewis, "Physical optics inverse diffraction," *IEEE Trans. Antennas Propag.* **AP-17,** 308–314 (May 1969).
19. P. L. Chu, "Optimal projection for multidimensional signal detection," *IEEE Trans. Acoust. Speech Signal Process.* **36**(5), 755–786 (May 1988).

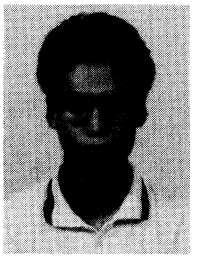

Jae-Ho Choi received the BSEE and MSEE and PhD (in computer engineering) degrees from North Carolina State University, Raleigh in 1985, 1988, and 1993, respectively. From 1990 to 1993, he has been with the Center for Systems Engineering, Research Triangle Institute, Research Triangle Park, NC, as a research consultant. Since 1993, he has been a member of the Department of Computer Engineering at Chonbuk National University, Chonju, Korea, where he is currently an assistant professor. His research interests are in the areas of target acquisition and tracking, color image processing, and video coding and communications. He is a member of IEEE, Sigma Xi, and KITE.

Sarah A. Rajala received the BSEE degree from Michigan Technological University, Houghton, in 1974, and the MS and PhD degrees in electrical engineering from Rice University, Houston, Texas, in 1977 and 1979, respectively. Since 1979, she has been a member of the Electrical and Computer Engineering Department at North Carolina State University, Raleigh, where she is currently a full professor. Professor Rajala has been an active researcher in the areas of target acquisition and tracking, motion estimation, color image processing, and time-varying image analysis with application to image coding.